CRYSTAL GROWTH & DESIGN

Article

pubs.acs.org/crystal

Growth Behavior of Monohydrocalcite ($CaCO_3 \cdot H_2O$) in Silica-Rich Alkaline Solution

Gan Zhang, José Manuel Delgado-López, Duane Choquesillo-Lazarte, and Juan Manuel García-Ruiz*

Laboratorio de Estudios Cristalográficos, Instituto Andaluz de Ciencias de la Tierra, CSIC-Universidad de Granada, Armilla, Granada, Spain

Supporting Information

ABSTRACT: Monohydrocalcite ($CaCO_3 \cdot H_2O$) has been crystallized in silica-rich alkaline water solution. The crystallization proceeds by a counterdiffusion method without the presence of any other additive except dissolved silica. The crystallization has been followed in situ by optical microscopy and Raman microspectroscopy, while the time evolution of the pH and the concentration of calcium and silica species in solution have also been followed either by in situ (pH) or ex-situ (calcium and silica) time-lapse analysis. The growth of monohydrocalcite particles occurs by different mechanisms that are related to the pH and the rate of pH change with time. The initial peanut-like crystal converts into an onion-like multilayered texture, which is built up by the alternation of loose layers and compact layers as a result of different levels of silica incorporation. A final silica-rich skin covers the hemisphere inhibiting the further growth of monohydrocalcite. When the silica skin fails to cover the whole surface of the hemisphere, a bulge of monohydrocalcite grows from the uncovered area until a new silica skin inhibits its growth except from a small uncovered area from which a new bulge forms. The iteration of this mechanism creates particles with caterpillar-like morphology. Our results show that silica plays a key role in the morphogenesis and texture of monohydrocalcite crystallization due to the coupled interaction between the reverse solubility of silica and carbonate versus pH.

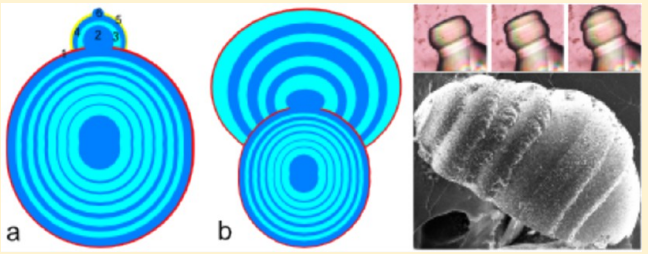

1. INTRODUCTION

Calcium carbonate is one of the most abundant materials in nature and is found both in geological and biological formation, and so it has aroused a great deal of interest and prompted in vitro studies throughout the recent past. Calcium carbonate occurs in a variety of polymorphic forms, of which three are anhydrous crystalline phases (calcite, aragonite, and vaterite), two well-defined hydrated crystalline phases (monohydrocalcite $CaCO_3 \cdot H_2O$ and ikaite $CaCO_3 \cdot 6H_2O$), and various amorphous forms.[1] Compared to the numerous studies on anhydrous calcium carbonate, the hydrated crystalline forms have been much less studied, certainly because they are poorly stable under ordinary conditions and easily transform into stable anhydrous phases such as calcite and aragonite.[2−4]

As a metastable hydrous calcium carbonate crystalline phase, monohydrocalcite (MHC) is rarely found in natural minerals compared to other anhydrous crystalline phases such as calcite and aragonite or even vaterite.[5] However, nowadays monohydrocalcite deserves more attention not only from a geological point of view but also due to its metastability and compositional similarity with hydrated amorphous calcium carbonate, which has recently been focused on as a key intermediate compound in biomineralization and biomimetic crystallization of calcium carbonate polymorphs.[6−8] The geological specimen of monohydrocalcite normally appears in magnesium-rich marine locations, where magnesium is generally incorporated into this phase in small quantities.[6,9] Biogenetic monohydrocalcite has also been found in organisms such as the otoliths of a tiger shark, the gall bladder of guinea pigs, and the calcareous corpuscles of parasitic worms.[10−12] In the laboratory, most experiments report that monohydrocalcite has been synthesized by the reaction of Ca^{2+} and CO_3^{2-} in the presence of Mg^{2+} when the Mg/Ca ratio was higher than 1, the results suggesting that Mg^{2+} played a key role in monohydrocalcite crystallization.[13,14] Furthermore, two articles report that monohydrocalcite can be synthesized without the presence of Mg^{2+} as an intermediate product and transformed into stable anhydrous calcium carbonate (calcite and aragonite) rapidly.[15,16] Because of its metastability and the high content of coprecipitated anhydrous forms (calcite, aragonite, or magnesium calcite), there is currently no such work reporting on the morphological evolution and growth behavior of monohydrocalcite crystallization.

In a previous study, we found a new route to produce monohydrocalcite in silica-rich alkaline solution without the presence of magnesium.[17] The precipitation procedure was done by the counterdiffusion method by the reaction of calcium chloride and sodium carbonate at room temperature and resulted in hemispherical multilayer formation made only of monohydrocalcite crystals. The results suggested that silica was

Received: July 17, 2014
Revised: December 26, 2014

DOI: 10.1021/cg5010775
Cryst. Growth Des. XXXX, XXX, XXX−XXX

a key factor in monohydrocalcite stabilization over a long period during the entire growth process (weeks). Considering this, even though both magnesium and silica are abundant inorganic species in natural minerals, while there is a huge amount of literature on the effect of magnesium on calcium carbonate crystallization,[18−21] there has been very little study of the effect of silica on calcium carbonate precipitation, although some reports have already indicated that silica could strongly affect calcium carbonate precipitation in crystal phases and morphogenesis.[22−27]

In the present work, we report the growth behaviors of monohydrocalcite in silica-rich alkaline solution. The growth history was followed by X-ray diffraction and in situ Raman microspectroscopy. The temporal evolutions of pH values and the concentrations of calcium and silica were analyzed by microelectrode and inductively coupled plasma optical emission spectrometry (ICP-OES), respectively. Meanwhile, energy dispersive X-ray spectroscopy (EDX) was combined with field emission scanning electron microscopy (FESEM) for the silica content analysis in the morphological observation, in a detailed examination of growth texture, in order to study the effect of different degrees of silica incorporation in monohydrocalcite crystallization and provide a special insight for explaining the relation between the different levels of silica coupling and the various growth behaviors of monohydrocalcite at different stages of crystallization.

2. MATERIALS AND METHODS

2.1. Crystallization of Calcium Carbonate. The crystallization of monohydrocalcite was carried out by counterdiffusion in a lab-made crystallization cell.[28] As the source of carbonate and silica, an alkaline silica gel containing sodium carbonate was set on the bottom of the cell, and a calcium chloride solution was injected into the top of the gel for the calcium carbonate precipitation. The initial experimental conditions were set up precisely according to our previous work.[17] First, 1.39 g of sodium silicate sol ($Na_2Si_3O_7$, 1−10 v/v, reagent grade, Sigma-Aldrich, replaced monthly) was mixed together with 9 mL of [0.05 M] sodium carbonate solution (Na_2CO_3, ≥99.0%, Sigma-Aldrich) by stirring for around 30 min. Then 3.5 mL of [1 M] HCl solution (analytical reagent, Fluka) was added and the mixture was stirred for another 30 s. The resulting gel precursor was transferred into the crystallization cell for gelling. The gelling time was 1 week, and the pH value was 10.5 ± 0.1 once the gel formed. Upon gelling, calcium chloride solution [0.05 M] ($CaCl_2$, ≥99.0%, Sigma-Aldrich) was injected into the cell on the top of the gel. Then the cell was blocked by vacuum grease again to prevent further diffusion of atmospheric carbon dioxide. The injection of calcium chloride was just considered as the time zero of the crystallization time scale. The diffusion of calcium chloride into the carbonate-containing gel and the diffusion of the carbonate into the calcium chloride solution provoked a chemical gradient temporally and spatially, which led to different concentrations of Ca^{2+} and CO_3^{2-} as well as Ca/CO_3 ratios, and to different supersaturation values with respect to $CaCO_3$ (both anhydrous and hydrated). Consequently, various morphologies and even different polymorphs appeared, as a function of time and location in the cell.

2.2. Phase Determination. The phase determination was carried out by X-ray diffraction and Raman microspectroscopy as reported in a previous paper.[17] In this paper, the structural homogeneity of the crystals was traced by mapping them with in situ and ex-situ Raman microscopy. Raman spectra were collected with a LabRAM-HR spectrometer attached to a microscope (Jobin-Yvon, Horiba, Japan). The excitation line was provided by a diode laser emitting at a wavelength of 532 nm, and a Peltier cooled charge-couple device (CCD) (1064 × 256 pixels) was used as detector. The optical microscope was equipped with 10× and 50× objectives (Olympus, Japan). The resulting data were imported into LabSpec Software (Horiba, Japan), and then the Raman map was reconstructed with a color code. Particularly in this work, the intensity of the peak appearing between 1080 and 1090 cm^{-1} (symmetric stretching of carbonate groups in calcite) was specified as red, the peak between 725 and 690 cm^{-1} was blue (symmetric bending of carbonate groups in calcite), and the intensity of the peak between 1060 and 1070 cm^{-1} (symmetric stretching of carbonate groups in monohydrocalcite) was green. Finally, the intensity of the Raman spectra was expressed by counts per second (cps).

2.3. Morphological Characterization. The growth of crystals was monitored by optical microscopy using a Nikon AZ100. At the early stage of the growth, a selected crystal was continuously recorded with a fixed time interval during crystallization. The resulting image sequences were imported into ImageJ software and converted into time-lapse videos. The growth rate of the crystals was determined by drawing a straight line from the core of the crystal to its growing front at different times and measuring the length of the lines. For the further study of the internal texture, the crystals were first enveloped by epoxy mounting media (Microtec) and warmed to 40 °C overnight to be completely enveloped. After that the enveloped samples were polished by sandpaper (Flexovit Grit P1200) to get smooth faces on the crystals, and then the resulting samples were studied by a Nikon Eclipse Ti inverted microscope.

Further morphological characterization was carried out by FESEM with an AURIGA (Carl Zeiss SMT) system. The crystals were extracted from the cell and washed with ultrapure water several times, dried at 40 °C overnight, and then coated by carbon for analysis. The energy dispersive X-ray spectroscopy (EDX) was associated with FESEM in the same system for the elemental analysis, in order to study the incorporation of the silica to the monohydrocalcite crystal during the different growth stages.

2.4. Time Evolution of pH and Concentrations of Calcium and Silica. The temporal evolution of the pH in solution during the crystallization was measured by inserting a microprobe (SENTRON micro electrode PEEK probe) in the crystallization cell. The probe was held in the liquid zone where the monohydrocalcite was expected to crystallize, and the hole was blocked again to prevent the further diffusion of atmospheric carbon dioxide during the crystallization. The pH values were thereby recorded automatically with an interval of 40 min.

The pH value in the solution was measured in situ during monohydrocalcite crystallization by microprobe. On the other hand, Ca^{2+} concentrations were determined by ICP-OES from a series of experiments with exactly the same initial conditions, and the results also provided the temporal evolution of the Ca^{2+} concentration in solution during the crystallization. In the multiple time-dependent profile of pH and Ca^{2+} concentration, the zero point was marked as soon as calcium chloride solution was added. For the experiments above, we also prepared a stock solution of silica sol to ensure the reproducibility of the gel feature for the investigation of the time evolution of Ca^{2+} concentration during the crystallization. The stock solution was distributed into 12 crystallization cells in order to prepare exactly the same initial conditions for monohydrocalcite crystallization in all the cells. All the crystallizations started at the same time, and the solutions were collected successively at different stages of the crystallization, and then the resulting solutions were analyzed in ICP-OES to measure the Ca^{2+} concentration. The same measurements were repeated with Silicon Standard for ICP (Sigma-Aldrich) to detect the time evolution of silica concentration.

3. RESULTS

3.1. Morphological Characterization. The growth of the crystals in the liquid zone of the crystallization cell was followed by time-lapse optical microscopy. Figure 1 shows the early stages (panel A) and further growth (panel B) of different crystals. The first precipitates observed under the microscope during the first 12 h of the experiment were tiny crystals (≤10 μm) identified as calcite by Raman spectroscopy (i.e., showing clear bands at 711 and 1086 cm^{-1}). From 12 to 36 h, peanut-

DOI: 10.1021/cg5010775
Cryst. Growth Des. XXXX, XXX, XXX−XXX

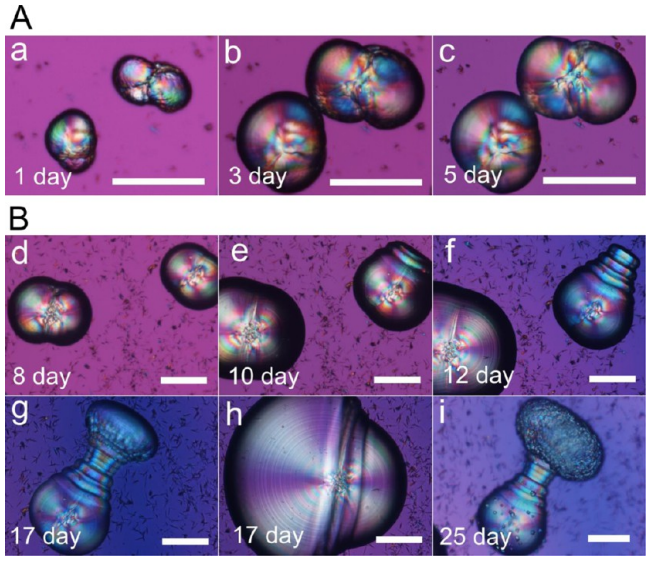

Figure 1. Optical microscopy images of the growth of hemispherical particles in the solution. The images were recorded by optical microscopy with crossed polarizers at first day (a), third day (b), fifth day (c), eighth day (d), 10th day (e), 12th day (f), 17th day (g and h), and 25th day (i). Images in panel A were collected from different regions from those depicted in panel B (scale bar: 50 μm).

shaped particles (Figure 1a) appeared in the solution. They stuck on the glass and then developed into a spherical shape with a diameter of around 50 μm in the third to fifth day (Figure 1b,c). Actually the shape developed is just a hemisphere because the particles always grow in contact with the glass wall of the crystallization cell. The hemisphere grew radially for 9 days to hundreds of micrometers in size (Figure 1d). This isotropic radial growth was commonly observed at this stage. However, in some cases (see Figure 1e,f) the crystal aggregate grew further anisotropically, and so changed the regular hemisphere into bizarre shapes (Figure 1g,h). The growth rate analyses also indicated that the later anisotropic growth was faster (1.22 μm/h) compared to the isotropic radial growth (0.43 μm/h and 0.67 μm/h, Supporting Information, Figure S1). During the third and fourth weeks of the crystallization, observation from optical microscopy revealed that the surface of the monohydrocalcite particles appeared covered by many tiny particles (Figure 1i). This high-density nucleation happened in a very short time (less than 1 day), and no further change was observed.

In addition to in situ optical microscopy, the growth of MHC particles was followed ex-situ by FESEM. Optical microscopy with crossed polarizers revealed that the initial peanut-like shape shows radial orientation of the crystals fibers (Figure 1a–d). This observation was also confirmed by FESEM studies (Figures 2a and 3a,b). The surface of this initial stage shows small particles of MHC with amorphous silica among them (Figure 2b). Once the particle grew bigger than 50 μm, the peanut-shape developed into a hemispherical shape (see FESEM images in Figure 2c).

After the gradual morphological transition from peanut to hemispherical shape, the monohydrocalcite crystal aggregate grew radially showing an onion-like concentric multilayered texture with the size of hundreds of micrometers. The FESEM

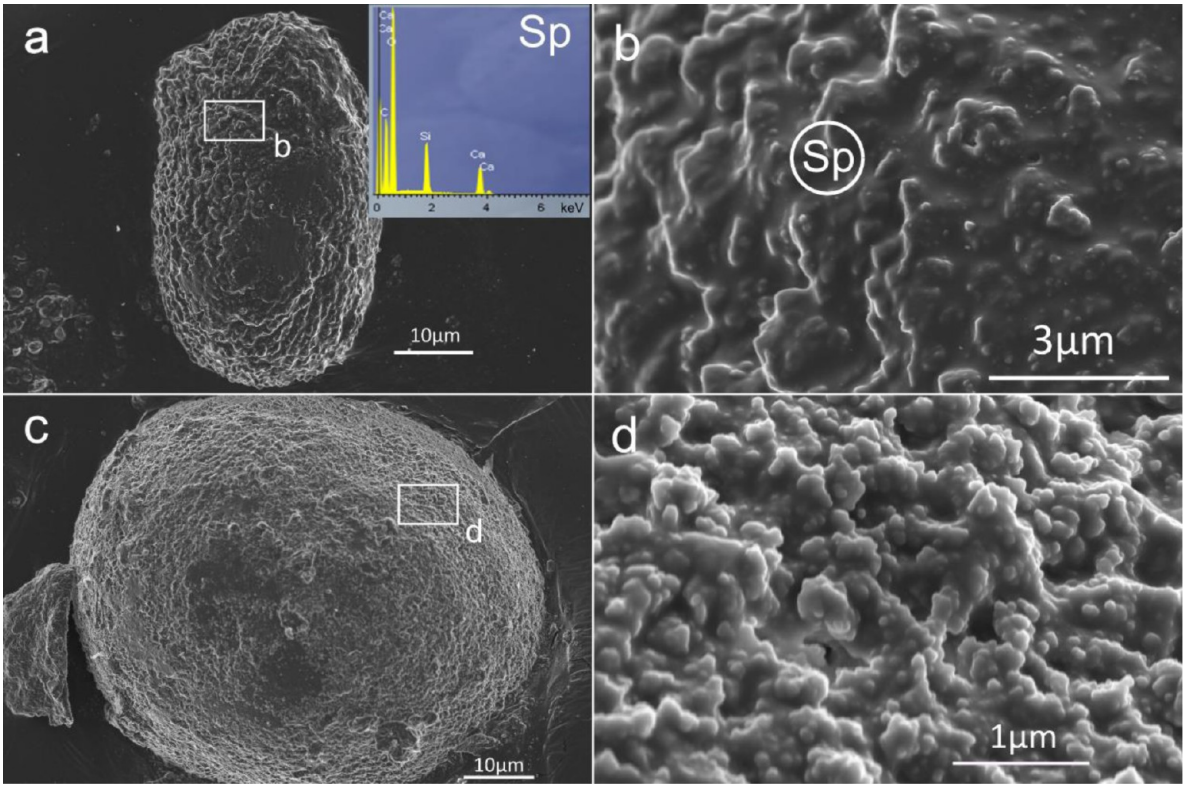

Figure 2. FESEM images of monohydrocalcite in the early stage of crystallization, from peanut shape to initial hemisphere: (a) peanut shape before the 36th hour (the inset shows an EDX spectrum of the white circle in b), (b) small particles and the precipitated silica of the peanut shape crystals (the white circle with Sp is the detecting area of EDX), (c) the initial hemisphere after the 36th hour of crystallization, (d) higher magnification images of the nanoparticles on the surface of the hemisphere.

DOI: 10.1021/cg5010775
Cryst. Growth Des. XXXX, XXX, XXX–XXX

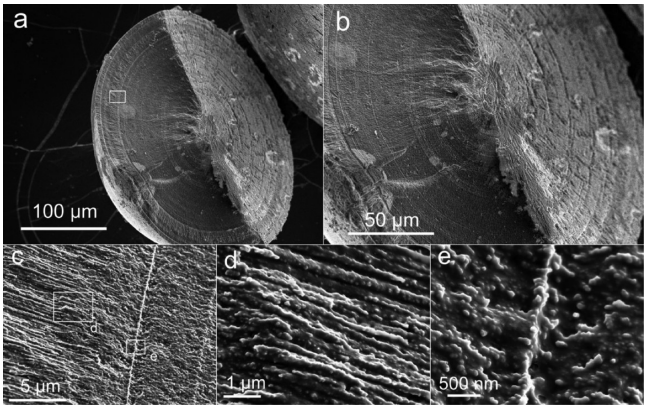

Figure 3. FESEM micrographs of monohydrocalcite: (a) a view of the cross-section of the hemisphere after 2 weeks crystallization; (b) enlarged view of the center area of the hemisphere in (a); (c) an enlarged view of the white rectangle in panel (a) within the multilayered region; (d) an enlarged view of the elongated crystals of the compact layer in the white rectangle in panel (c) showing that they are formed by co-oriented nanorods along the elongation of the fiber; (e) an enlarged view of the loose layer (band) in the white rectangle in panel (c).

textural study shows that the multilayered texture was built up by the alternation of a compact layer and loose layers (Figure 3).[17] These layers are made by nanorods elongated along the *c*-axis with a typical width of about 50 nm (Figure 3d). According to the different level of compactness and degree of co-orientation of the nanorods, the concentric layers were classified into two types, namely, compact layer and loose layer (Figure 3c). The compact layers are formed by radially arranged fiber-like crystallites that are built up by nanorods with high co-orientation (Figure 3c,d). This kind of layer alternates with the loose layers, which contain similar nanorods but with lower density and degree of co-orientation. The onion-like texture made by the alternation of layers (Figure 3c) suggests an oscillatory growth behavior.[22,29,30] Notably, the thickness of the layers was at the micron scale but varied largely from the center to the edge of the whole crystal aggregate, and typically, newly forming compact layers became thinner. A continuous thin (less than one micrometer thick) layer covering the whole onion-like multilayered texture, which we call skin,[17] can also be noted. This skin is made of monohydrocalcite nanospheres with a diameter of around 100 nm, and the EDX results indicated high silica content, either within or in between the nanoparticles. Figure 4 shows EDX spectra collected at different zones of the crystal aggregate. Spectrum Sp 01 demonstrates the high silica contents in the skin, while the fraction of silica in multilayered texture was much lower (spectra Sp 03 and Sp 04). Particularly, the small clusters on the multilayered texture, which was produced by the high-density nucleation described before, also show a high content of silica (spectrum Sp 02), but not as great as that of the skin.

The silica skin forms during the third or fourth week of the crystallization experiment. When this skin completely covers the crystal aggregate, there is no further growth, and it remains hemispherical in shape. However, if the skin does not cover the entire surface, a singular phenomenon takes place. Then, the uncovered region of monohydrocalcite continues to grow forward as a protuberance or bulge as shown in the optical micrographs of Figure 1f–h and FESEM views in Figures 5 and 6. This growth also takes place in an oscillatory mode in the form of new pairs of compact layers (Figure 5e) and loose layers (Figure 5b,f). High-resolution images in Figure 5b,e also show that the crystals maintain the same orientation from the previous uncovered region. Actually, they grow further, changing the orientation to adopt a hemispherical shape as well, invading neighboring areas covered by the silica skin (see Figure 5d). This first bulge is then covered by a new silica skin that inhibits its further growth (Figure 5d) except from a small, uncovered region from which a second bulge starts to form with the same texture. This kind of growth repeats several times until the silica skin covered the whole surface of the n-bulge to fully inhibit further growth of the monohydrocalcite crystal aggregate. The final shape resembles a caterpillar.

Optical microscopy observations revealed a high-density nucleation as the final step of monohydrocalcite crystallization

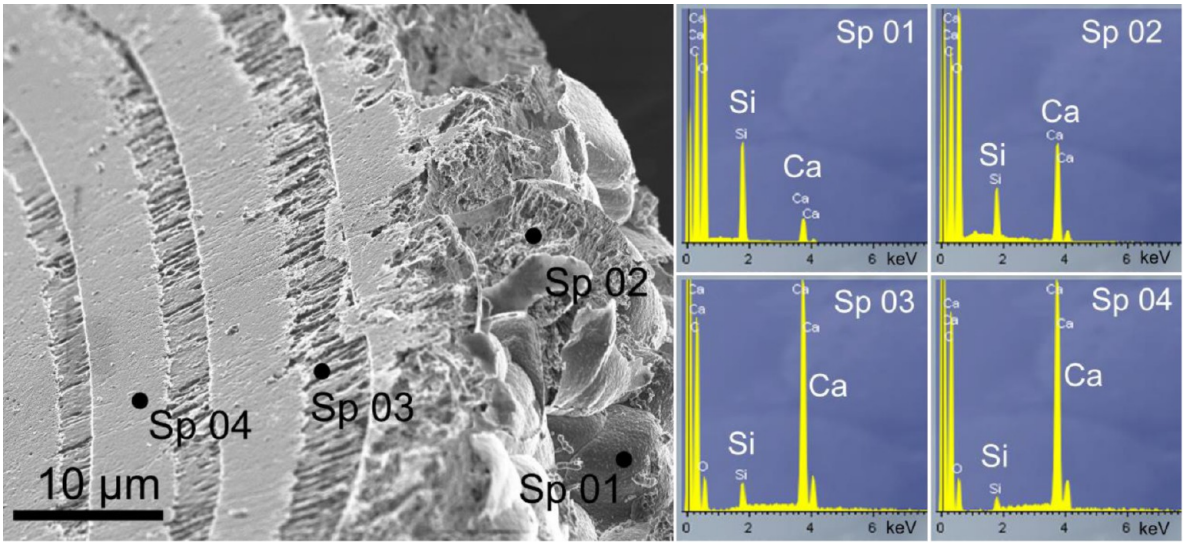

Figure 4. FESEM micrograph of monohydrocalcite and the corresponding EDX spectra collected from different locations on the crystal surface: the so-called skin (Sp 01, Si/Ca = 4.2:1), the small particle clusters from the high-density nucleation (Sp 02, Si/Ca = 1:2.4), the loose (Sp 03, Si/Ca = 1:10.8) and compact (Sp 04, Si/Ca = 1:21.4) layers of the onion-like multilayered texture.

DOI: 10.1021/cg5010775
Cryst. Growth Des. XXXX, XXX, XXX–XXX

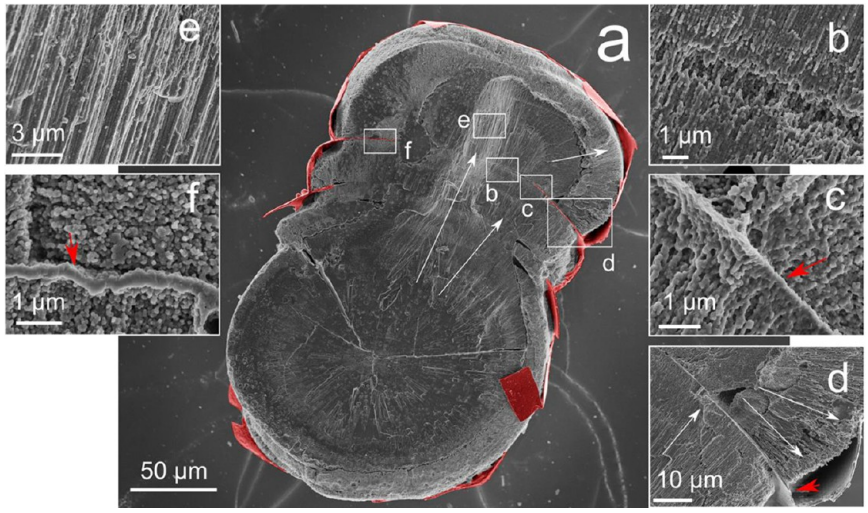

Figure 5. FESEM images of monohydrocalcite in an irregular shape after 4 weeks crystallization (a). Micrographs (b), (c), (d), (e), and (f) show higher magnification of (a) in different positions. The silica skin is colored by red in (a) and marked by red arrows in (c), (d), and (f). The different orientations of the nanorods are marked by white arrows in (a) and (d).

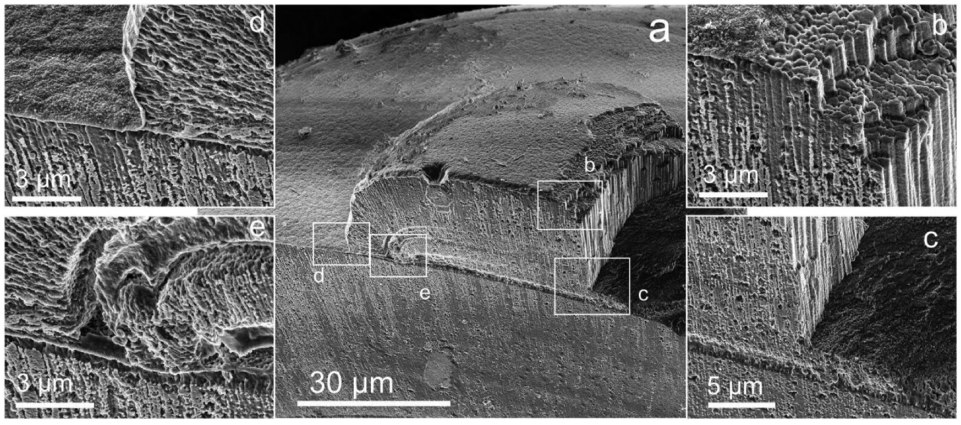

Figure 6. FESEM micrographs of monohydrocalcite showing the early growing stage of a bulge (after 2 weeks crystallization): (a) the bulge forms by further growth of the monohydrocalcite layers not covered by the skin of silica; (b) the texture of the growth front of the new layers; (c) the silica skin of the original hemisphere and the initial growing front from the uncovered region; (d) the silica skin of the original hemisphere and the silica skin of the new layers; (e) the new multilayered texture developed over the initial hemisphere.

(Figure 1i). The crystal aggregate becomes covered by a large amount of small particles. The FESEM results (Figure 7) indicate that these particles are made by a disordered aggregation of MHC nanoparticles of 50−100 nm in size (Figure 7d) which is covered by a skin of silica (Sp 02 in Figure 4), and they look like particles with a typical size of 10 μm (Figure 7b). Occasionally, these clusters are also covered by a continuous silica skin and exhibited an irregular shape as shown in the right side of Figure 7a.

3.2. Phase Determination by Raman Microspectroscopy. In a previous study,[17] it has already been proven by X-ray synchrotron diffraction that the hemisphere was made of monohydrocalcite. The in situ Raman spectra performed in this study demonstrates that monohydrocalcite was the initial phase from the early stage of the crystallization (the peanut-shaped particles), and there was no phase transformation during the whole process. In this study, we have used 2D X-Y Raman mapping to analyze the structural homogeneity, particularly for the small clusters from the high-density nucleation. The intensity of the peak appearing between 1080 and 1090 cm^{-1} (symmetric stretching of carbonate groups in calcite) was labeled as red in the Raman map and the intensity of the peak between 1060 and 1070 cm^{-1} (symmetric stretching of carbonate groups in monohydrocalcite) was labeled green.[9,17,31] The monohydrocalcite sample was extracted from the cell when the entire crystallization ceased after 4 weeks. Figure 8 shows the Raman map (inset a) and the optical micrograph of the same zone (inset b) as well as the Rama spectrum of the zone marked with a white square in inset a. The irregular border in the micrograph shows the presence of the small clusters, and the Raman spectrum of the white square in this border is in good agreement with the spectrum of monohydrocalcite.[9] The results show that the Raman map is completely green colored, and this confirms that the entire crystal aggregate is monohydrocalcite, as well as the small cluster from high-density nucleation.

3.3. Time Evolution of the pH and the Ca^{2+} Concentration. Figure 9 shows the time evolution of the pH and Ca^{2+} concentration during a crystallization experiment. A significant pH increase in the first 12 h is clearly observed, which fits the crystallization of the time of the tiny calcite according to the optical microscopy observation. From the 12th

DOI: 10.1021/cg5010775
Cryst. Growth Des. XXXX, XXX, XXX−XXX

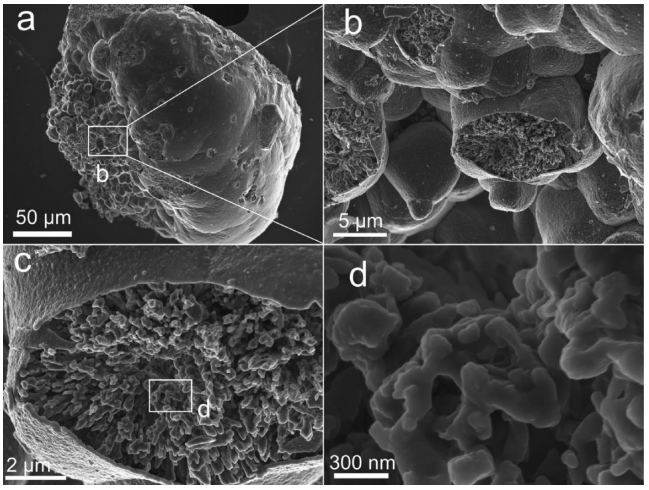

Figure 7. FESEM images of monohydrocalcite after high-density nucleation: (a) hemispherical monohydrocalcite which is completely covered by small nanoparticles, and the nanoparticles developed into many small clusters on the surface and then covered by silica skin; (b) a detailed view of the small spheres; (c) the skin and the internal texture of small cluster; (d) the nanoparticles of the small clusters in high magnification view.

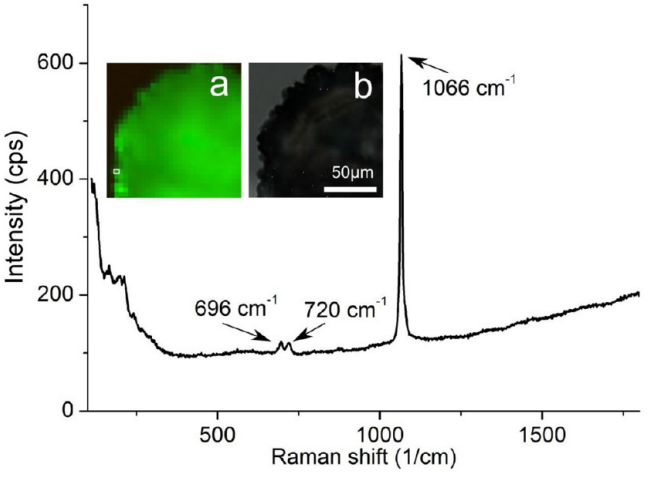

Figure 8. Raman spectrum of selected monohydrocalcite obtained upon cessation of growth collected from the white square in a. Inset (a): Raman map; inset (b): optical microscopy image of the region analyzed by Raman.

to the 24th hours, which is considered as the early stage of monohydrocalcite crystallization, the pH is still sharply increasing but slower than just at the beginning. Notably, there is no more nucleation of monohydrocalcite in the liquid zone after 48 h when the pH is around 9.3. Therefore, we infer the initial pH value for monohydrocalcite nucleation is around 9.3, and the crystallization of calcite ceases completely from then. During the development of the initial peanut shape to hemisphere (between 24 and 96 h) the pH slowly increases from 9.4 to 9.7, accordingly. However, after 96 h, the pH stays constant around 9.7 showing small shifts in the pH profile, which is considered as the stage of the oscillatory growth (see Figure S4 in Supporting Information). And this oscillatory growth forms the concentric sublayered texture in the hemispherical monohydrocalcite, or in other words, the onion-like multilayered texture as shown in the inset in Figure 9 (at pH 9.7, from 96 to 168 h). The pH value keeps increasing

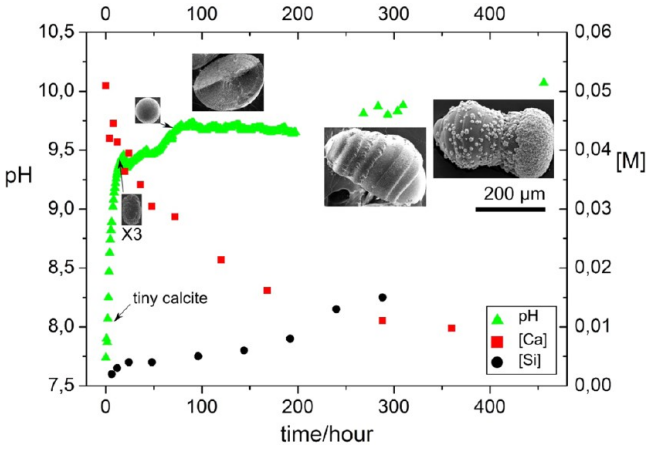

Figure 9. Time evolution of the pH and the concentrations of Ca and Si (left). The insets show the typical morphologies of monohydrocalcite at the different growing stages. All the images retain the same scale bar (200 μm), except the one at 36 h and pH 8.7, which is three times enlarged.

to 9.8 at the end of the second week, then the onion-like multi layered texture is covered by the silica skin, and the further growth of monohydrocalcite is blocked. Meanwhile, as we have described above, due to the interaction between the growth of monohydrocalcite and the inhibition of silica skin, the crystal grows from the uncovered region and develops new layers, changing the hemisphere into an irregular shape (inset in Figure 9, at pH 9.8, the second week). The pH increases to 9.9 or 10.0 after the second week, and the high-density nucleation occurs on the surface of the crystal aggregate. When the pH is higher than 10.0 in the third week (456 h in Figure 9), the high-density nucleation stops, and there is no more change in either the morphology of the crystal or the pH value in solution, and hence we consider this stage to be the end of the crystallization.

4. DISCUSSION

The precipitation of calcium carbonate in silica-rich alkaline solution is controlled by the following reactions:

$$Ca^{2+} + CO_3^{2-} \leftrightarrows CaCO_3 \quad (1)$$

$$HCO_3^- + H_2O \leftrightarrows H_3O^+ + CO_3^{2-} \quad (2)$$

$$Si(OH)_4 \leftrightarrows Si(OH)_3^- + H_3O^+ \text{ at pH 9.0} \quad (3)$$

$$Si(OH)_3^- \leftrightarrows Si(OH)_2^{2-} + H_3O^+ \text{ at pH 10.7} \quad (4)$$

Rather than a classical single pot reaction of mixed solutions, our crystallization experiment must be analyzed as a continuous nonequilibrium system where mass as transport is controlled by diffusion, and the above reactions depends on the variation of the pH value as a function of time. The starting pH value of the silica gel is around 10.5, while the starting value of the calcium chloride solution added on top of the gel is 6.3. As shown in Figure 9, this pH value increases quickly due to the upward diffusion of the alkaline silica species from the gel. The increase in pH ultimately provokes the supersaturation of the top solution with respect to calcium carbonate due to the shift of the CO_2 speciation equilibrium toward CO_3^{2-}. Tiny calcite crystals are the first phase to precipitate after 2 h when the pH value is about 8.0. Monohydrocalcite starts to form at pH 9.4 and does so as the only calcium carbonate phase forming until

DOI: 10.1021/cg5010775
Cryst. Growth Des. XXXX, XXX, XXX−XXX

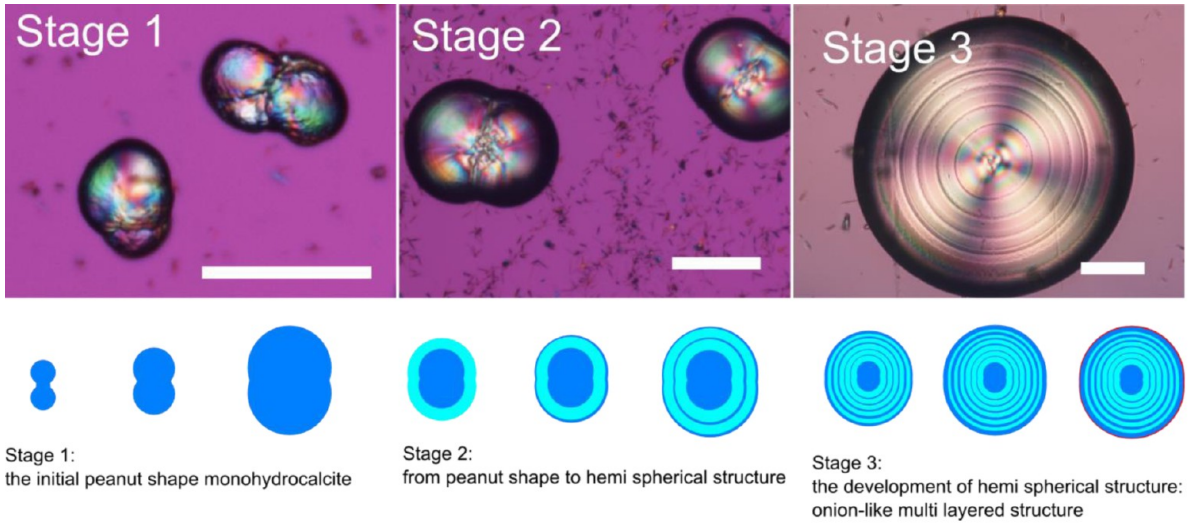

Figure 10. Scheme of the monohydrocalcite crystallization during the first 3 weeks. Stage 1: first 2 days crystallization; Stage 2: after 1 week crystallization; Stage 3: after 2 weeks of crystallization. The optical microscopic images are collected from different crystals (scale bar: 50 μm).

the end of the experiment. The nucleation of monohydrocalcite takes place at a rate of pH change of 2.1 pH units/day, which means a high rate of supersaturation of calcium carbonate. Consequently, the texture of the initial core appears made by disordered nanocrystals showing an irregular peanut-like shape (Figure 3b). The transition from this disordered starting phase to the hemispherical shape occurs at pH 9.7 with a slower rate of change of pH of 0.13 units per day. Later, the precipitation of the multilayered region with highly ordered textures of the loose and compact layer occurs at constant pH value of the bulk. As the system is closed to interaction with the atmosphere, the driving force for the precipitation of carbonate and silica must be due to small variations of pH at the local growth front driven by the self-coupling rate of carbonate and silica precipitation[32] and by daily variations in laboratory temperature.

The whole crystal growth process appears to be the result of the aggregation of nanoparticles of MHC with a degree of co-orientation that depends on the rate of carbonate production that in turn depends on the rate of increase in pH, as described above. The nanoparticles forming the aggregates do not display clear faceted shapes. The inhibition of the growth and the rounded morphology are most probably due to the effect of adsorbed silica on the surfaces of MHC nanoparticles.[32−34] While the MHC mineral structures grow in the bulk of the top solution of $CaCl_2$, the silica gel behaves as a continuous source of dissolved silica pumped to the top solution as $H_3SiO_4^-$ and $H_2SiO_4^{2-}$species. Thus, the experiment can be understood as the interplay of the kinetics of silica and carbonate precipitation as the result of the reverse solubility of barium carbonate and silica versus pH. The presence of soluble silica has a key effect on monohydrocalcite crystallization. As shown in Figure 9, when the initial monohydrocalcite core develops into the regular hemisphere at pH around 9.7, the pH value decreases due to the fast precipitation of calcium carbonate. This decrease in pH in turn increases the local supersaturation of silica around the growing monohydrocalcite crystals, provoking silica coprecipitation that inhibits the growth of monohydrocalcite nanoparticles but not its nucleation. As a result of the precipitation of silica, the pH increases again reducing the amount of silica available to coprecipitate with calcium carbonate in the advancing growing front. It is important to notice that at the value of pH at which this stage of the growth occurs (pH 9.7) the dependence of the solubility of silica with respect to pH is very high. It means that, unlike at smaller pH values, the sensitivity of silica solubility to small changes in pH is very high, which makes two different ratios of calcium carbonate to silica precipitation possible. This difference is responsible for the different local crystalline textures observed in FESEM as compact layer and loose layer, with high and low content of coprecipitated silica, as shown in Figures 3 and 4. Later, the system is almost exhausted in carbonate but silica continues to be pumped from the gel so that the concentration of silica increases as shown in Figure 11. Then a "skin" of high silica content is precipitated as shown by the FESEM images and EDX analysis in Figure 4.

This morphological and textural evolution is shown diagrammatically in Figure 10. The mineral deposition monohydrocalcite starts with peanut shapes shown in Figures 1a and 2a, most probably as the result of the conversion of an initial splitting single crystal into a dumbbell-like shape (stage 1 in Figure 10).[35−37] Then, the continuous spherulitic radial growth gradually changes the morphology from peanut shape to a hemispherical shape (stage 2 in Figure 10). In this stage, the growth of the compact layers and loose layers occurs, the thickness of the compact layer (cyan layer in Figure 10) being bigger than that of the loose layer (blue layer in Figure 10), because the amount of dissolved silica is still small at these relatively low values of pH. Stage 3 in Figure 10 occurs at higher pH, when the compact layers and loose layers become a similar thickness producing an onion-like multi layered texture, as shown in FESEM in Figure 3a. As the pH slowly increases, there is more dissolved silica in the solution, and the thickness of the loose layer becomes bigger while that of the compact layer becomes smaller. At pH higher than 9.7, the silica skin forms covering the surface of the crystal aggregate (thin red layer in the last inset of Stage 3 in Figure 10) inhibiting further growth of monohydrocalcite. Later, both silica concentration and pH increase (close to pH 10.2, see Figure 9) due to the continuous flow upward of silica molecules from the gel. This combined increment of carbonate and silica provoke large and fast coprecipitation of MHC and silica, in the form of tiny

DOI: 10.1021/cg5010775
Cryst. Growth Des. XXXX, XXX, XXX−XXX

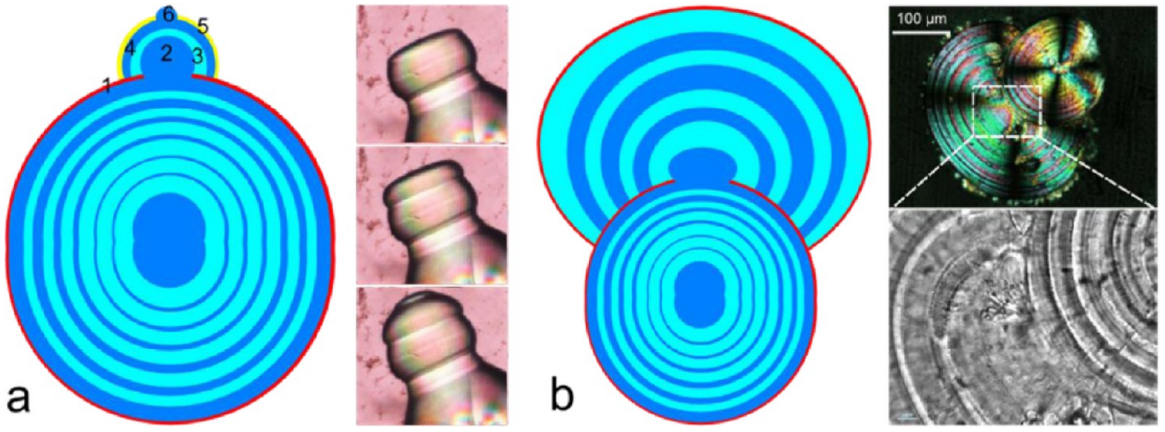

Figure 11. (a, b) Growth mechanism of the caterpillar shape. The photographs in inset a are from the selected frames in the video in Supporting Information; the colored photograph in inset b is recorded by optical microscope, and the monochrome is from the selected frame in the video in Supporting Information. The video is recorded by a Nikon Eclipse Ti inverted microscope, and the selected frame is overturned in order to be consistent with the colored photograph from optical microscopy.

crystals with much higher silica content compared to the compact layers and loose layers (see Figure 4 Sp 02).

4.1. Caterpillar Morphology. In some cases the silica skin does not completely cover the hemisphere. This allows the growth of new layers of monohydrocalcite from the uncovered region of the onion-like multilayered texture, thus breaking its hemispherical shape. This occurs as shown diagrammatically in Figure 11 and illustrated in Figure 6. Note that the growth of new layers on the section of the crystal aggregate not covered by the silica skin occurs in a radial way keeping the orientation of the previous layers as described in the Results. Optical microscopic photographs in the inset of Figure 11a and the video of crystal growth in Supporting Information clearly show this growth behavior. New pairs of compact (cyan) layer and loose (blue) layer form, and they growth isotropically to shape the bulge hemispherically. After that, a new silica skin forms on the surface of the new layer, blocking further growth of MHC except for a small uncovered area from which a new bulge forms. The iteration of this process of bulge formation shapes the original hemisphere like a caterpillar.

5. CONCLUSION

Self-assembled onion-like layered hemispheres of monohydrocalcite were grown and stabilized in silica-rich alkaline solution by the counterdiffusion method without any other additive. In situ study by Raman microspectroscopy demonstrates that monohydrocalcite was the nucleating phase and that no phase transformation occurs during the whole process.

Our results reveal that silica species in the alkaline solution have a critical effect on both the morphology and texture of monohydrocalcite crystals forming the crystal aggregate. It has been experimentally demonstrated by in situ measurement of pH values, and ex-situ silica and calcium concentrations that the time evolution of pH is the key variable controlling the ratio of the cocrystallization of silica and carbonate. The growth occurs always by the aggregation of nanoparticles of MHC. The degree of order of the aggregation depends on the rate of creation of nanoparticles, which depends on the rate of increase of pH. We show that the three different observed growth stages correlate with the rate of supersaturation of MHC and the sensitivity of silica solubility to the change in pH. Layers of different textures and $CaCO_3/SiO_2$ ratios are alternatively formed at constant pH of the bulk of the solution. Finally, the whole growth history ended with a silica skin. When the silica skin does not totally cover the crystal aggregate, bulges of layered MHC grow from the uncovered region that tend also to adopt a hemispherical shape. A succession of these protuberances may take place until the system extenuates, or the silica skin totally covers the last protuberance. Under these circumstances the final shape looks like a caterpillar.

■ ASSOCIATED CONTENT

Supporting Information

The growth rate of monohydrocalcite hemispheres, video of the growth of new bulge from the onion-like multilayered texture of monohydrocalcite, the FESEM images of new bulges of multilayered texture of monohydrocalcite, scanning video in *Z*-axis by inverted microscope of new bulge after crystallization, the X-Y 2D Raman map of selected monohydrocalcite that enclosed calcite in the center, and the time evolution of the pH during the crystallization of monohydrocalcite (from 60 to 200 h). This material is available free of charge via the Internet at http://pubs.acs.org.

■ AUTHOR INFORMATION

Corresponding Author

*E-mail: juanmanuel.garcia@csic.es.

Notes

The authors declare no competing financial interest.

■ ACKNOWLEDGMENTS

The authors would like to thank the Ministerio de Economía y Competitividad (MINECO) for the financial support through the Consolider-Ingenio 2010 project "Factoría Española de Cristalización" and the projects CGL2010-16882 and CGL2010- 12099. We also acknowledge the ERC-ADG Grant 340863-PROMETHEUS. G.Z. and J.M.D.L. also acknowledge the Consejo Superior de Investigaciones Científicas for the JAE predoctoral grant and postdoctoral JAE-DOC contract, respectively, both within the program "Junta de Ampliación de Estudios" and cofinanced with the European Social Fund (ESF). The authors also acknowledge Alicia González Segura for her support with the FESEM and EDX analysis, and Mónica Pineda Dorado for her support with the ICP-OES analysis.

DOI: 10.1021/cg5010775
Cryst. Growth Des. XXXX, XXX, XXX−XXX

REFERENCES

(1) Meldrum, F. C. *Int. Mater. Rev.* **2003**, *48*, 187−224.
(2) Brooks, R.; Clark, L. M.; Thurston, E. F. *Philos. Trans. R. Soc. London* **1950**, *243*, 145−167.
(3) Hull, H.; Turnbull, A. G. *Geochim. Cosmochim. Acta* **1973**, *37*, 685−694.
(4) Kamiya, K.; Sakka, S.; Terada, K. *Mater. Res. Bull.* **1977**, *12*, 1095−1102.
(5) Kimura, T.; Koga, N. *J. Phys. Chem. A* **2011**, *115*, 10491−10501.
(6) Neumann, M.; Epple, M. *Eur. J. Inorg. Chem.* **2007**, *2007*, 1953−1957.
(7) Addadi, L.; Raz, S.; Weiner, S. *Adv. Mater.* **2003**, *15*, 959−970.
(8) Gower, L. B. *Chem. Rev.* **2008**, *108*, 4551−4627.
(9) Tlili, M. M.; Amor, M. B.; Gabrielli, C.; Joiret, S.; Maurin, G.; Rousseau, P. *J. Raman Spectrosc.* **2002**, *33*, 10−16.
(10) Carlström, D. *Biol. Bull.* **1963**, *125*, 441−463.
(11) Skinner, H. C. W.; Osbaldiston, G. W.; Wiener, A. N. *Am. Mineral.* **1977**, *62*, 273−277.
(12) Señorale-Pose, M.; Chalar, C.; Dauphin, Y.; Massard, P.; Pradel, P.; Marín, M. *Exp. Parasitol.* **2008**, *118*, 54−58.
(13) Fukushi, K.; Munemoto, T.; Sakai, M.; Yagi, S. *Sci. Technol. Adv. Mater.* **2011**, *12*, 064702.
(14) Rodriguez-Blanco, J. D.; Shaw, S.; Bots, P.; Roncal-Herrero, T.; Benning, L. G. *Geochim. Cosmochim. Acta* **2014**, *127*, 204−220.
(15) Jiménez-López, C.; Caballero, E.; Huertas, F. J.; Romanek, C. S. *Geochim. Cosmochim. Acta* **2001**, *65*, 3219−3231.
(16) Stepkowska, E. T. *J. Therm. Anal. Calorim.* **2005**, *80*, 727−733.
(17) Zhang, G.; Delgado-López, J. M.; Choquesillo-Lazarte, D.; García-Ruiz, J. M. *CrystEngComm* **2013**, 6526−6532.
(18) Loste, E.; Wilson, R. M.; Seshadri, R.; Meldrum, F. C. *J. Cryst. Growth* **2003**, *254*, 206−218.
(19) Reddy, M. M.; Nancollas, G. H. *J. Cryst. Growth* **1976**, *35*, 33−38.
(20) Raz, S.; Weiner, S.; Addadi, L. *Adv. Mater.* **2000**, *12*, 38−42.
(21) Sánchez-Navas, A.; Martín-Algarra, A. n.; Rivadeneyra, M. a. A.; Melchor, S.; Martín-Ramos, J. D. *Cryst. Growth Des.* **2009**, *9*, 2690−2699.
(22) Dominguez Bella, S.; Garcia-Ruiz, J. M. *J. Mater. Sci.* **1987**, *22*, 3095−3102.
(23) Voinescu, A. E.; Kellermeier, M.; Bartel, B.; Carnerup, A. M.; Larsson, A.-K.; Touraud, D.; Kunz, W.; Kienle, L.; Pfitzner, A.; Hyde, S. T. *Cryst. Growth Des.* **2008**, *8*, 1515−1521.
(24) Kellermeier, M.; Melero-García, E.; Glaab, F.; Klein, R.; Drechsler, M.; Rachel, R.; García-Ruiz, J. M.; Kunz, W. *J. Am. Chem. Soc.* **2010**, *132*, 17859−17866.
(25) Imai, H.; Terada, T.; Miura, T.; Yamabi, S. *J. Cryst. Growth* **2002**, *244*, 200−205.
(26) Imai, H.; Terada, T.; Yamabi, S. *Chem. Commun.* **2003**, 484−485.
(27) Kellermeier, M.; Melero-García, E.; Kunz, W.; García-Ruiz, J. M. In *Kinetics and Thermodynamics of Multistep Nucleation and Self-Assembly in Nanoscale Materials*; John Wiley & Sons, Inc.: New York, 2012; pp 277−307.
(28) Melero-García, E.; Santisteban-Bailón, R.; García-Ruiz, J. M. *Cryst. Growth Des.* **2009**, *9*, 4730−4734.
(29) Shore, M.; Fowler, A. D. *Can. Mineral.* **1996**, *34*, 1111−1126.
(30) Putnis, A.; Fernandez-Diaz, L.; Prieto, M. *Nature* **1992**, *358*, 743−745.
(31) Kontoyannis, C. G.; Vagenas, N. V. *Analyst* **2000**, *125*, 251−255.
(32) García-Ruiz, J. M.; Melero-García, E.; Hyde, S. T. *Science* **2009**, *323*, 362−365.
(33) Kunz, W.; Kellermeier, M. *Science* **2009**, *323*, 344−345.
(34) Bittarello, E.; Roberto Massaro, F.; Aquilano, D. *J. Cryst. Growth* **2010**, *312*, 402−412.
(35) Busch, S.; Dolhaine, H.; DuChesne, A.; Heinz, S.; Hochrein, O.; Laeri, F.; Podebrad, O.; Vietze, U.; Weiland, T.; Kniep, R. *Eur. J. Inorg. Chem.* **1999**, *1999*, 1643−1653.
(36) Beck, R.; Andreassen, J.-P. *Cryst. Growth Des.* **2010**, *10*, 2934−2947.
(37) Gránásy, L.; Pusztai, T.; Tegze, G.; Warren, J. A.; Douglas, J. F. *Phys. Rev. E: Stat., Nonlinear, Soft Matter Phys.* **2005**, *72*, 011605.

DOI: 10.1021/cg5010775
Cryst. Growth Des. XXXX, XXX, XXX−XXX